Pertanika J. Sci. & Technol. 32 (3): 1427 - 1438 (2024)

PERTANIKA JOURNALS

SCIENCE & TECHNOLOGY

Journal homepage: http://www.pertanika.upm.edu.my/

Modeling of Light Lifting Robotic Arm

Norfarahana Adibah Raffie[1], Noor Hafizah Amer[1,2]*, Syed Mohd Fairuz Syed Mohd Dardin[1], Khisbullah Hudha[1] and Saiddi Ali Firdaus Mohamed Ishak[1]

[1]Department of Mechanical Engineering, Faculty of Engineering, National Defense University of Malaysia, Sg. Besi Army Camp, 57000 Kuala Lumpur, Malaysia
[2]Centre of Defense Research and Technology, National Defense University of Malaysia, Sg. Besi Army Camp, 57000, Kuala Lumpur, Malaysia

ABSTRACT

Robotic arms are often chosen as the primary manipulator for teleoperated robots specializing in executing tasks that require high skills from humans. The optimization of robotic arm design has been studied extensively using various types of optimization algorithms. However, studies validating and optimizing robotic arms with a high degree of freedom (DOF) using co-simulation techniques are scarce. This study presents the validation and modeling of a five-DOF robotic arm by observing the torques produced by each robotic arm joint using the co-simulation method between Solidworks and Simscape Multibody. The system is modeled in a Solidworks environment with full freedom and overall configurations. The model is then exported to Simscape Multibody for modeling processes. Several validation processes were conducted to validate the Simscape Multibody by comparing torques produced from the three-DOF robotic arm in Simscape with three DOF dynamic equations. Further validation was conducted using coordinate geometry of the end effector position in Solidworks, Simscape, and mathematical geometry models. The proposed co-simulation model agrees with the mathematical model with an average error of 7.6%. This study will likely provide a new approach to the co-simulation technique for systems with a high degree of freedom.

Keywords: Design optimization, lagrange equation, Simscape Multibody, Simulink, Solidworks

ARTICLE INFO

Article history:
Received: 16 August 2023
Accepted: 21 November 2023
Published: 04 April 2024

DOI: https://doi.org/10.47836/pjst.32.3.25

E-mail addresses:
farahanaraffie@gmail.com (Norfarahana Adibah Raffie)
noorhafizah@upnm.edu.my (Noor Hafizah Amer)
syedfairuz@upnm.edu.my (Syed Mohd Fairuz Syed Mohd Dardin)
k.hudha@upnm.edu.my (Khisbullah Hudha)
saiddi@upnm.edu.my (Saiddi Ali Firdaus Mohamed Ishak)
*Corresponding author

INTRODUCTION

It is well known that assessing in a hazardous environment poses a huge challenge to humans. The chance of an accident has become the main motivation for continuously studying robotics as a human assistant. In carrying out a task, some robots may be equipped with controllable arms that could reach a distance range with moveable

ISSN: 0128-7680
e-ISSN: 2231-8526

claws to grip any desired object. Programmed robotic arms that can be operated remotely are among various industries' most common human replacements. A wide range of robotic arms can be observed in the manufacturing and production industries, where programmable robotic arms perform tasks such as drilling, machining, and assembling. Apart from the industrial field, robotic arms are also used for tasks in hazardous environments to manage safety risks to human personnel. Examples of the utilization of a robotic arm in a hazardous environment can be observed in Pioneer, a teleoperated robot used to explore the Chernobyl power plant in the 1986 disaster, and LOUIE 1, which was deployed at Three Mile Island in 1979 (Tsitsimpelis et al., 2019). Pioneer has a robotic arm that collects the radioactive material remaining from the blast. Meanwhile, LOUIE 1 was assigned as a surveying robot.

The efficiency of the robotic arm lies in how well it is being designed. Therefore, many studies have focused on the design optimization of the robotic arm by first developing an analytical and simulation model of the system. It is usually beneficial to be used in the preliminary design stages to finalize the dimensions and concept designs. It will save time and cost to develop the final product. An industrial robotic arm was developed using the ANSYS Shape Optimization analysis (Bugday & Karali, 2019). The study used a model developed in ANSYS to optimize and analyze mechanical properties for each shape selection of the arm. In addition, a modification was proposed to modify the robotic arm kinematics from an originally non-redundant manipulator by adding virtual joints, making the robotic arm kinematically redundant, and introducing free motion of the mechanism (Maaroof et al., 2022). This mechanical redundancy allows researchers to visualize the robot configuration and optimize specific structural configuration variations.

Another research study has been conducted by Santosh et al. (2022) to develop a small-scale robotic arm using Creo Parametric software and Ansys Workbench. The paper focused on optimizing the design by observing the effect of changing the materials in the Ansys Workbench Finite Element Method under different loading conditions applied in the analysis. This similar process in robotic arm development could also be observed from a study by Ali et al. (2023) that used Solidworks to design the robotic arm for lightweight lifting and export it to Ansys Workbench to analyze the robotic arm. It was found that Finite Element Method (FEM) in the Ansys Workbench could provide feasible data in developing the robot arm for both studies. Yang and Hein (2023) suggested a training program that used machine learning to predict the weight of the objects lifted by the robot arm by observing the torques produced by the robot. The study promotes the ability of machine learning to grasp a larger variety of data as a tool in developing and optimizing robotic arms. However, the proposed method will depend on the data for one particular system. Another system will have to be developed with perhaps a different machine learning technique as proposed.

There are a few other recent studies on modeling robotic arms for further optimization (Seth et al., 2022; Seki et al., 2021). Among these, most designs were generic with two

to three degrees of freedom (DOF). More DOFs will pose different challenges and constraints on the modeling process. Those studies that consider more DOFs considered methods that will apply only to the specific design. By combining finite element analysis and dynamic analysis in MATLAB/Simulink, more complicated problems can be solved. Several researchers have explored the co-simulation approach between the FEA software and MATLAB/Simulink to allow more dynamic analyses. Among these, no proposal on the robotic arms modeling with more than three DOFs using co-simulation between FEA and MATLAB/Simulink software has been proposed.

In addressing this gap, this paper outlines the proposal to model and validate the design of a five-DOF robotic arm using the co-simulation technique between Solidworks and Simscape module in MATLAB/Simulink. This co-simulation will consider the more complicated DOFs as well as an easier transition to be used for other systems. This paper will discuss a co-simulation approach to model the considered system, which can be beneficial for numerical optimization works and applicable to various systems. It includes the derivation of three and five DOFs robotic arm Lagrangian mathematical model to verify the proposed co-simulation method, followed by the verification process to validate the proposed approach.

METHODS

Design of Robotic Arm

A robotic arm with five DOFs has been designed in a previous study (Raffie et al., 2021) based on the product design specification required. Five concept designs of the robotic arm have been generated and evaluated to select the finalized robotic arm for the light lifting task. The robotic arm will have one twisting joint, three rotating joints, and one prismatic joint. Four stepper motors will actuate these joints for rotational motion, and a brushless linear motor will act as an actuator for linear motion for the fifth link. The finalized design of the robotic arm considered in this study is shown in Figure 1.

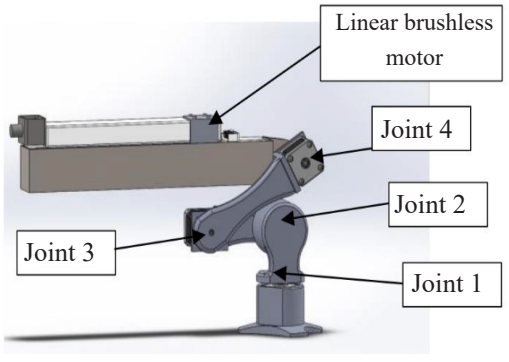

Figure 1. The finalized design of the five-DOF robotic arm

Development of Mathematical Model

Development of the Three-DOF Model. The Lagrange equation is an alternative to the Newton-Euler equation often used to describe the motion of systems with many DOFs and is more advantageous when the systems have more derivable forces

obtained from potential energy (Lee, 2006). The Lagrange equation is one of the most powerful tools in deriving equations of motion for a complicated system (Stutts, 2017). Equation 1 is using this approach.

$$\frac{d}{dt}\frac{\partial L}{\partial \dot{q}_i} - \frac{\partial L}{\partial q_i} = Q_i, \qquad i = 1, \dots, n \tag{1}$$

Where q_i is the generalized coordinate, $\dot{q}_i$ is the generalized velocity, and Q_i is the generalized external force in the system. Here, L is the Lagrangian term, which consists of the total kinetic energy within K and total potential energy, P, within the moving system, described in Equation 2.

$$L = K - P \tag{2}$$

In deriving the Lagrange equation for the three-DOF robotic arm shown in Figure 2, the generalized coordinate for the system can be derived as shown in Equations 3 and 4.

$$x_i = L_i \cos\theta_i \tag{3}$$

$$y_i = L_i \sin\theta_i \tag{4}$$

Here, x_i and y_i are the displacements in the x-axis and y-axis. L_i is the length of each robotic arm link, and θ_i is the angle of the link from the x-axis. From the geometry expression, kinetic and potential energy can be obtained. Hence, the Lagrangian as in Equation 5.

$$L = \sum \frac{1}{2} m V_i^2 + \sum \frac{1}{2} I \dot{\theta}_i^2 + \sum mgy_i \tag{5}$$

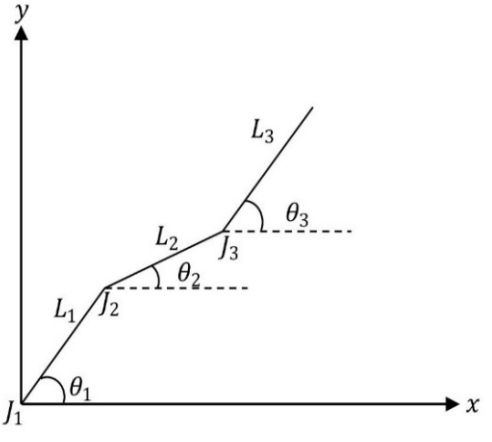

Figure 2. Three-DOF robotic arm free body diagram

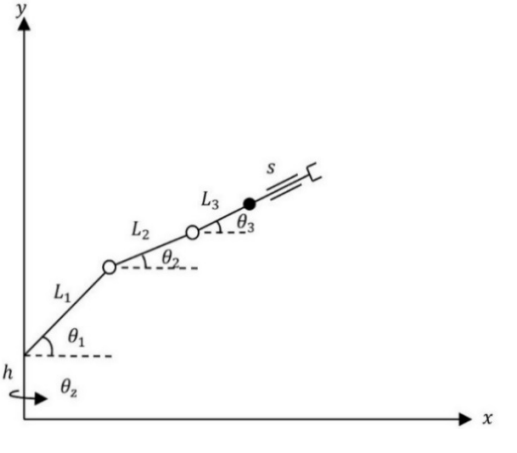

Figure 3. Five-DOF diagram

Since there are three generalized coordinates for the robotic arm, the Lagrange equation can be expressed as Equations 6, 7, and 8.

$$\frac{d}{dt}\frac{\partial L}{\partial \dot{\theta_1}} - \frac{\partial L}{\partial \theta_1} = \mathrm{T}_1 \quad [6]$$

$$\frac{d}{dt}\frac{\partial L}{\partial \dot{\theta_2}} - \frac{\partial L}{\partial \theta_2} = \mathrm{T}_2 \quad [7]$$

$$\frac{d}{dt}\frac{\partial L}{\partial \dot{\theta_3}} - \frac{\partial L}{\partial \theta_3} = \mathrm{T}_3 \quad [8]$$

The final form of the governed equations for the three-DOF robotic arm can be obtained as in Equations 9, 10 and 11.

$$\mathrm{T}_1 = L_1\big(M_1 g cos(\theta_1) + M_2 g\cos(\theta_1) + M_3 g cos(\theta_1) + L_2 M_2 \dot{\theta_2}\dot{\theta_1}\sin(\theta_1 - \theta_2) + L_2 M_3 \dot{\theta_2}\dot{\theta_1}\sin(\theta_1 - \theta_2) + L_3 M_3 \dot{\theta_3}\dot{\theta_1}\sin(\theta_1 - \theta_3)\big) \quad [9]$$

$$\mathrm{T}_2 = L_2 M_2 g cos(\theta_2) + L_2 M_3 g cos(\theta_2) - L_1 L_2 M_2 \dot{\theta_1}\dot{\theta_2}(\sin(\theta_1 - \theta_2)) - L_1 L_2 M_3 \dot{\theta_1}\dot{\theta_2}(\sin(\theta_1 - \theta_2)) + L_2 L_3 M_3 \dot{\theta_2}\dot{\theta_3}(\sin(\theta_2 - \theta_3)) = 0 \quad [10]$$

$$\mathrm{T}_3 = L_3 M_3 g cos\theta_3 - L_1 L_3 M_3 \dot{\theta_3}\dot{\theta_1}\sin(\theta_1 - \theta_3) - L_2 L_3 M_3 \dot{\theta_3}\dot{\theta_2}\sin(\theta_2 - \theta_3) = 0 \quad [11]$$

Development of the Five-DOF Model. A similar derivation method was used to generate a mathematical model for the five-DOF of the proposed robotic arm using the Lagrange equation. The derivation of torque equations using the Lagrangian was conducted based on the free-body diagram of the five DOFs shown in Figure 3. Here, the same coordinates are used as in Equations 3 and 4. The final form of the derived equations can be observed from Equations 17, 18, 19, 20 and 21. There would be an addition to the velocity equation for the fifth link as the distance of the link can vary depending on the controller's desire due to its translational motion. The derivation for kinetic energy for the fifth link is complicated due to the sliding distance that is not constant. Hence, the displacement notation and velocity in *the x* and *y* axes can be observed from the following Equations: 12, 13, 14, 15, and 16.

$$x_5 = s\cos\theta_3 \quad [12]$$

$$y_5 = s\sin\theta_3 \quad [13]$$

$$\dot{x}_5 = \dot{s}\cos\theta_3 - s\dot{\theta}_3 sin\theta_3 \quad [14]$$

$$\dot{y}_5 = \dot{s} sin\theta_3 + s\dot{\theta}_3 cos\theta_3 \quad [15]$$

$$\text{Therefore, } K_5 = \frac{1}{2}m_5(\dot{s}^2 + s^2\dot{\theta}_3^2) \quad [16]$$

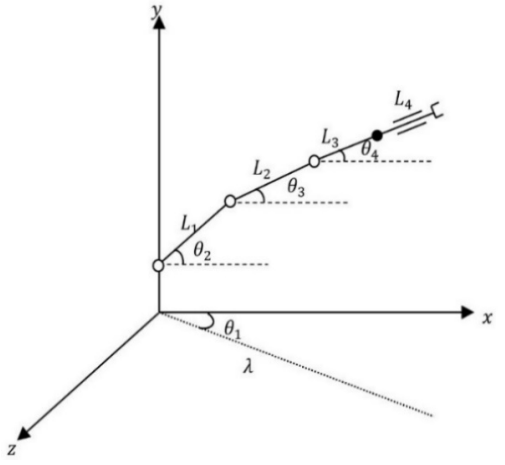

Figure 4. Free body diagram of the five-DOF robotic arm for coordinate geometry model

The generalized coordinates for all five DOFs of the Lagrange equation can be expressed as follows: Equations 17, 18, 19, 20, and 21.

$$\frac{d}{dt}\frac{\partial L}{\partial \dot{\theta}_1} - \frac{\partial L}{\partial \theta_1} = \mathrm{T}_1 \quad [17]$$

$$\frac{d}{dt}\frac{\partial L}{\partial \dot{\theta}_2} - \frac{\partial L}{\partial \theta_2} = \mathrm{T}_2 \quad [18]$$

$$\frac{d}{dt}\frac{\partial L}{\partial \dot{\theta}_3} - \frac{\partial L}{\partial \theta_3} = \mathrm{T}_3 \quad [19]$$

$$\frac{d}{dt}\frac{\partial L}{\partial \dot{\theta}_4} - \frac{\partial L}{\partial \theta_4} = \mathrm{T}_4 \quad [20]$$

$$\frac{d}{dt}\frac{\partial L}{\partial \dot{s}} - \frac{\partial L}{\partial s} = F_s \quad [21]$$

Development of the Geometric Model. The simulation model will also be validated using a geometric model that describes the coordinate of the end effector upon rotational input in each joint. The geometric model of the five-DOF robotic arm can be derived as Equations 22, 23, 24 and 25 using the same notation in Figure 3.

$$Y_{eff} = h + L_1 sin\theta_2 + L_2 sin\theta_3 + (L_3 + L_4) sin\theta_4 \quad [22]$$

$$\lambda = L_1 cos\theta_2 + L_2 cos\theta_3 + (L_3 + L_4) cos\theta_4 \quad [23]$$

$$X_{eff} = \lambda cos\theta_1 \quad [24]$$

$$z_{eff} = \lambda sin\theta_1 \quad [25]$$

Where Y_{eff}, X_{eff} and Z_{eff} are the coordinates of the end effector at each axis x, y, and z, respectively. The coordinates of the end effector were observed from equations with three different robot arm trajectories, where the free-body diagram for the five-DOF robot arm could be observed in Figure 4.

Development of the Simscape Model

The 3D model of the robotic arm was then imported into the MATLAB Simscape Multibody environment. Simscape Multibody features that can convert rigid subassemblies in Solidworks into a rigid body in Multibody became the greatest advantage in minimizing the time consumption for the user in modeling CAD in Simulink. In this study, both robotic arms with three DOFs (based on Ramish et al., 2016) and five DOFs (based on the finalized design in Figure 1) were developed in Solidworks before being converted into the

Simscape multibody model. The co-simulation was carried out in the SOLIDWORKS 2020 and MATLAB Simulink version R2021b using solver ode45 and 0.01s step size settings. Further investigations on the effect of software versions and simulation settings yield indifferent results, meaning the proposed approach can be carried out on different versions.

RESULTS AND ANALYSIS

Validation of the Simscape Multibody Simulation Method

Stage 1 Validation of the Three-DOF. A previous study by Ramish et al. (2016), which outlined the validation process for a three-DOF robotic arm, was taken as a reference for the validation process. Based on the paper, the same motion input was supplied to each link of the proposed robotic arm. Using MATLAB/Simulink and Simscape Multibody, all modeling was simulated with the acceleration and trajectory inputs (Figure 5) within the duration of 1 second. The simulation showed a comparison of joint torques between the mathematical model from the previous study and the Simulink Multibody model (Figure 6). The percentage of error of the results was calculated to analyze the difference between the measured value from the Simulink Multibody and previous data. The purpose of finding the percentage of error, obtainable using Equations 26 and 27, is to observe the closeness of the measured torque from the multibody with the torque in the previous study. The calculated percentage of errors can be observed in Table 1.

$$\text{Percentage of error} = \frac{\left|\mathrm{T_{multibody}} - \mathrm{T_{previous}}\right|}{\mathrm{T_{max}}} \times 100\% \quad [26]$$

$$RMS = \sqrt{\frac{(x_1^2 + x_2^2 \ldots + x_n^2)}{N}} \quad [27]$$

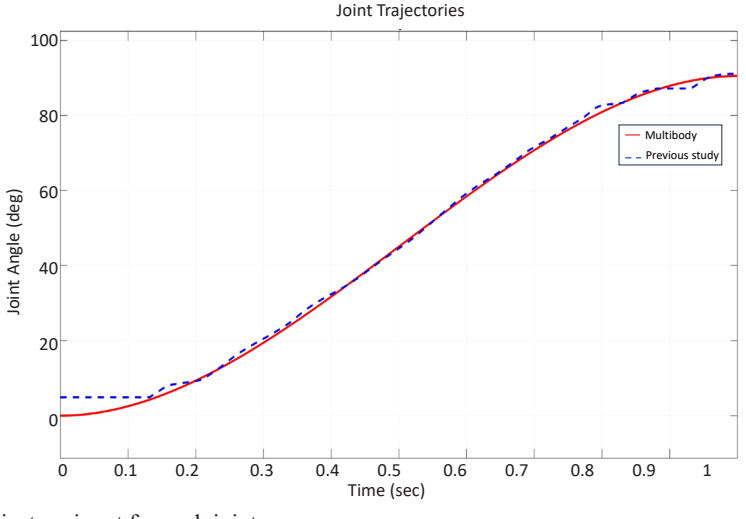

Figure 5. Trajectory input for each joint

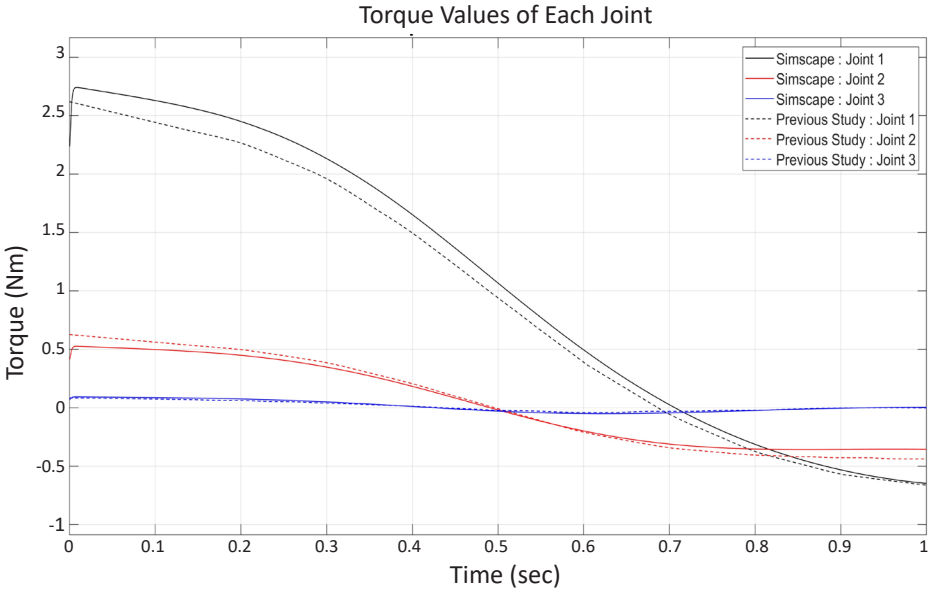

Figure 6. Torques produced by the Lagrange equation and Simscape Multibody

Stage 2 Validation of the Five-DOF. In this stage, the Simscape model of the proposed five-DOF robotic arm will be verified against the Lagrange mathematical equation with five systems based on the robotic arm in Figure 1. The trajectory inputs of the validation were generated using the cubic polynomial trajectory planning method (Guan et al., 2005). The cubic trajectory for the robotic arm can be observed in Equations 28, 29 and 30, where $q(t)$, $q'(t)$ and $q''(t)$ are the joint variables for the joint angle, angular velocity, and angular acceleration of the joint, which vary with time, t.

$$q(t) = a_0 + a_1 t + a_2 t^2 + a_3 t^3 \quad [28]$$

$$q'(t) = a_1 + 2a_2 t + 3a_3 t^2 \quad [29]$$

$$q''(t) = 2a_2 + 6a_3 t \quad [30]$$

The joint trajectory is shown in Figure 7, where the joint angles were set from 0° at the initial position and 50° at the final position within 5 seconds, while the fifth link was actuated to be fully extended within the same time set. These settings are based on the product design specification for the robotic arm to ensure efficient response (arm should be fully extended within 5 seconds) and workspace limitation (extended arm should not block LIDAR and remain within designated dimensions). The generated torques from the Simulink Multibody model were then observed and compared with the torque values produced from the mathematical model (Figure 8). The percentage errors between them were calculated and tabulated in Table 1 and Table 2, which shows a decent comparison between the two methods. The average error for the five DOFs model validation can be determined from values in Table 2, which is 7.6%. It shows that the variation between the

proposed Simscape model and the mathematical model is well within the acceptable limit of experimental accuracy (10%). The large error for Joint 1 (32.16 %) can be attributed to its ability to withstand more mass than the other joints, as shown in Figure 1. It will give rise to more resistance to motion between joints in the actual system that were not fully captured in the mathematical equations.

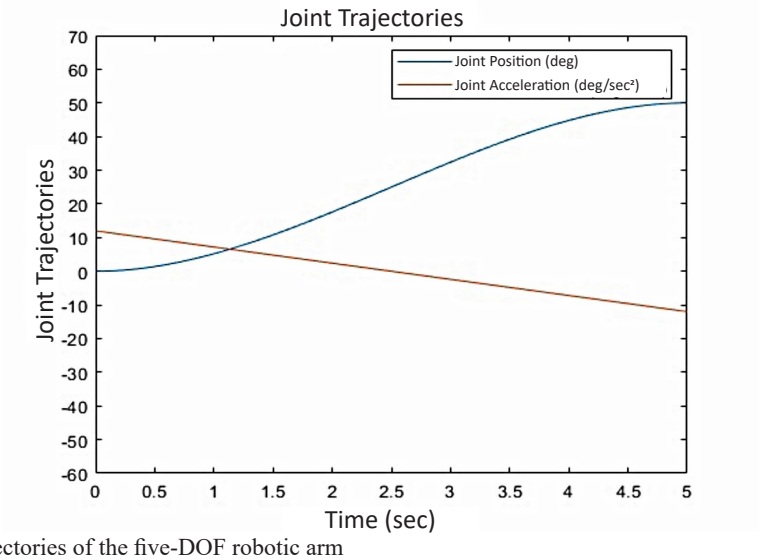

Figure 7. Trajectories of the five-DOF robotic arm

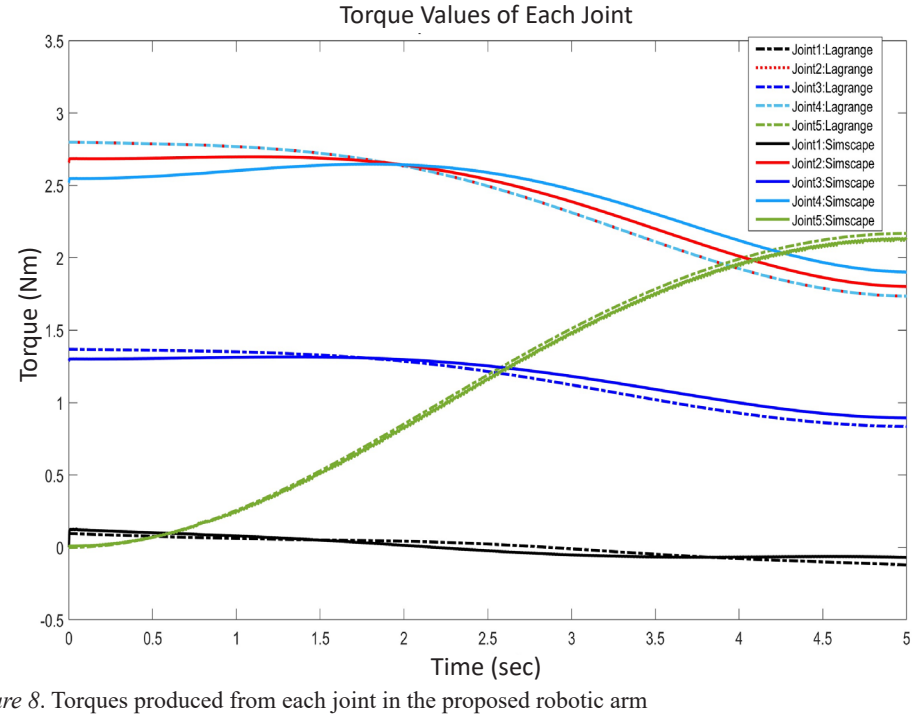

Figure 8. Torques produced from each joint in the proposed robotic arm

Table 1
Percentage error of each joint for the three-DOF

	Percentage of Error (%)
Joint 1	32.16
Joint 2	15.14
Joint 3	9.22

Table 2
RMS error (RMSE) for five-DOF system

	RMS Percentage Error (%)
Joint 1	24
Joint 2	3
Joint 3	4
Joint 4	6
Joint 5	1
AVERAGE	7.6

Table 3
The angle of each joint for different positions

	Position 1	Position 2	Position 3
Joint 1	0	0	45
Joint 2	0	45	45
Joint 3	0	45	45
Joint 4	0	45	45

Table 4
Coordinate end effector (in meters) for different positions

	Position 1	Position 2	Position 3
Simscape model	[0.67,0.16, 0.03]	[0.30,0.71, 0.03]	[0.19,0.71, 0.25]
Geometric model	[0.66,0.16, 0]	[0.35, 0.73, 0]	[0.18, 0.73, 0.30]

Stage 3 Validation of Coordinate Geometric. The Simscape simulation model is further validated using a geometric model of the derived robotic arm. This step acts as another validation layer to verify the model against theoretical values before further simulation. This time, the position of the robotic arm's end effector will be verified. Three different cases were shown, which indicate different orientations of the arm: Position 1 (initial arm position with all joints at 0°), Position 2, and Position 3 (extended arm with all joints at maximum angle). The subsequent joint angle for each orientation and position is shown in Table 3. The end coordinate will be recorded from the Simscape and mathematical geometric models. Table 4 presents the obtained coordinates. Each set of values corresponds to the *X*, *Y*, and *Z* coordinates of the arm's end effector from the system origin.

DISCUSSION

Validation results for the three-DOF robotic arm in Figures 5 and 6 proved that the robotic arm model developed in the Simscape Multibody (by converting the CAD design of the robotic arm in Solidworks into the MATLAB Simscape Multibody) could produce a similar torque response compared to the experimental torque values from a previous study. By deriving a Lagrangian model based on the previous method, the five-DOF validation showed that the torque responses from the mathematical and Simscape models have a similar trend throughout the simulation. Some slight differences can be observed for joints two, three, and four in the five-DOFs system validation, which can be attributed to the various interactions and friction not modeled by the Lagrangian mathematical model. The

validation and percentage errors in Table 2 show that the Simscape model could produce a torque value close to the torques from the mathematical model for the five-DOF robotic arms, with an average of 7.6% deviations in all joints.

Further validation using the geometric model in Table 4 shows that the Simscape model managed to predict the end effector positions well within 0.05 m of *X*, *Y*, and *Z* coordinates. The difference can be attributed to the exclusion of friction and interaction effects in the mathematical model. Despite the errors in Joint 1, all the other joints were recorded as acceptable, which fulfills the main focus of this study, which is to model the end effector located at the rod on Joints 4 and 5. In addition, a very significantly lower error on Joint 5 (1%), which only has translational motion, shows that the error is small on the most important location of interest. In conclusion, the proposed co-simulation method between Simscape and Solidworks has been developed and validated using multiple verification methods. The overall difference between the simulated and theoretical responses is well within satisfactory range. This study will move into applying the proposed model to optimize the design of robotic arms in the future.

ACKNOWLEDGMENTS

This research has received support and funding from the Malaysian Ministry of Higher Education through the Fundamental Research Grant Scheme (FRGS/1/2021/TK02/UPNM/02/2) and Universiti Pertahanan Nasional Malaysia (UPNM) under the internal grant of UPNM/2019/CHEMDEF/ST/6.

REFERENCES

Ali, Z., Sheikh, M. F., Al Rashid, A., Arif, Z. U., Khalid, M. Y., Umer, R., & Koç, M. (2023). Design and development of a low-cost 5-DOF robotic arm for lightweight material handling and sorting applications: A case study for small manufacturing industries of Pakistan. *Results in Engineering*, *19*, 101315. https://doi.org/10.1016/j.rineng.2023.101315

Bugday, M., & Karali, M. (2019). Design optimization of industrial robot arm to minimize redundant weight. *Engineering Science and Technology, an International Journal*, *22*(1), 346–352. https://doi.org/10.1016/j.jestch.2018.11.009

Guan, Y., Yokoi, K., Stasse, O., & Kheddar, A. (2005). On robotic trajectory planning using polynomial interpolations. In *2005 IEEE International Conference on Robotics and Biomimetics - ROBIO* (pp. 111-116). IEEE. https://doi.org/10.1109/ROBIO.2005.246411

Lee, W. H. (2006). Lagrangian method. *Computer Simulation of Shaped Charge Problems*, 5-30. https://doi.org/10.1142/9789812707130_0002

Maaroof, O. W., Dede, M. İ. C., & Aydin, L. (2022). A robot arm design optimization method by using a kinematic redundancy resolution technique. *Robotics*, *11*(1). https://doi.org/10.3390/robotics11010001

Raffie, N. A., Amer, N. H., Dardin, S. M. F. S. M., Hudha, K., & Ishak, S. A. F. M. (2021). Preliminary concept modelling, evaluation and selection of robotic arm for light lifting application. In *2021 7th International*

Conference on Mechanical Engineering and Automation Science (*ICMEAS*) (pp. 178-183). IEEE. https://doi.org/10.1109/ICMEAS54189.2021.00043

Ramish, Hussain, S. B., & Kanwal, F. (2016). Design of a 3 DoF robotic arm. In *2016 Sixth International Conference on Innovative Computing Technology* (*INTECH*) (pp. 145-149). IEEE. https://doi.org/10.1109/INTECH.2016.7845007

Santosh, L. P. S., Mishra, N., Mahanta, S. S. A., Dharmarajan, V., Varma, S. K., & Shoor, S. (2022). Design and analysis of a robotic arm under different loading conditions using FEA simulation. *Materials Today: Proceedings*, *50*, 759–765. https://doi.org/10.1016/j.matpr.2021.05.457

Seki, H., Nakayama, S., Uenishi, K., Tsuji, T., Hikizu, M., Makino, Y., & Kanda, Y. (2021). Development of assistive robotic arm for power line maintenance. *Precision Engineering*, *67*, 69-76. https://doi.org/10.1016/j.precisioneng.2020.09.006

Seth, A., Kuruvilla, J. K., Sharma, S., Duttagupta, J., & Jaiswal, A. (2022). Design and simulation of 6-DOF cylindrical robotic manipulator using finite element analysis. *Materials Today: Proceedings*, *62*, 1521-1525. https://doi.org/10.1016/j.matpr.2022.02.365

Stutts, D. S. (2017). *Analytical Dynamics: Lagrange's Equation and its Application – A Brief Introduction*. Missouri University of Science and Technology.

Tsitsimpelis, I., Taylor, C. J., Lennox, B., & Joyce, M. J. (2019). A review of ground-based robotic systems for the characterization of nuclear environments. *Progress in Nuclear Energy*, *111*, 109-124. https://doi.org/10.1016/j.pnucene.2018.10.023

Yang, F., & Hein, J. E. (2023). Training a robotic arm to estimate the weight of a suspended object. *Device*, *1*(1). https://doi.org/10.1016/j.device.2023.100011